Spin Relaxation Benchmarks and Individual Qubit Addressability for Holes in Quantum Dots

Lawrie, W. I.L.; Hendrickx, N. W.; van Riggelen, F.; Russ, M.; Petit, L.; Sammak, A.; Scappucci, G.; Veldhorst, M.

DOI
10.1021/acs.nanolett.0c02589

Publication date
2020

Document Version
Final published version

Published in
Nano Letters

NANO LETTERS

pubs.acs.org/NanoLett

Letter

Spin Relaxation Benchmarks and Individual Qubit Addressability for Holes in Quantum Dots

W. I. L. Lawrie,* N. W. Hendrickx, F. van Riggelen, M. Russ, L. Petit, A. Sammak, G. Scappucci, and M. Veldhorst*

Cite This: *Nano Lett.* 2020, 20, 7237−7242

Read Online

ACCESS | Metrics & More | Article Recommendations | Supporting Information

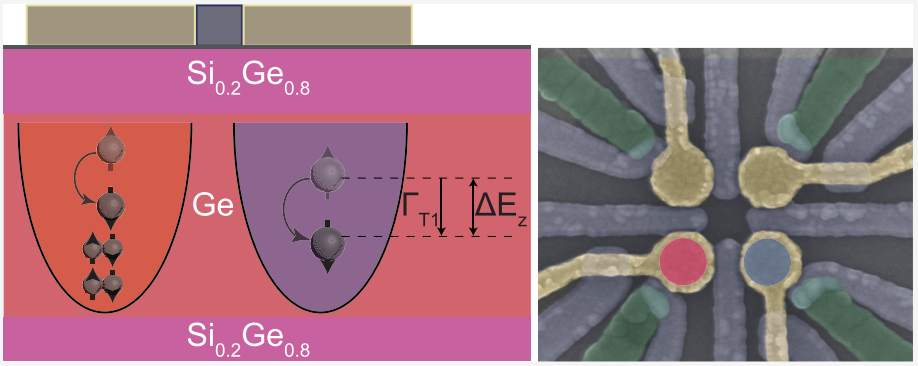

ABSTRACT: We investigate hole spin relaxation in the single- and multihole regime in a 2 × 2 germanium quantum dot array. We find spin relaxation times T_1 as high as 32 and 1.2 ms for quantum dots with single- and five-hole occupations, respectively, setting benchmarks for spin relaxation times for hole quantum dots. Furthermore, we investigate qubit addressability and electric field sensitivity by measuring resonance frequency dependence of each qubit on gate voltages. We can tune the resonance frequency over a large range for both single and multihole qubits, while simultaneously finding that the resonance frequencies are only weakly dependent on neighboring gates. In particular, the five-hole qubit resonance frequency is more than 20 times as sensitive to its corresponding plunger gate. Excellent individual qubit tunability and long spin relaxation times make holes in germanium promising for addressable and high-fidelity spin qubits in dense two-dimensional quantum dot arrays for large-scale quantum information.

KEYWORDS: *Germanium, quantum dots, spin relaxation, qubits*

Qubits based on spin states are well-established candidates for quantum information processing.[1] Pioneering studies were conducted on low-disorder gallium arsenide heterostructures,[2,3] but quantum coherence remained limited due to hyperfine interaction with nuclear spins. These interactions can be eliminated by using isotopically enriched group IV semiconductors as the host material.[4] In silicon, this has led to landmark achievements, such as extremely long quantum coherence[5] and relaxation times,[6] single qubit gates with fidelities beyond 99.9%,[7,8] execution of two-qubit gates,[9,10] quantum algorithms,[11] and the operation of single qubit rotations[12] and two-qubit logic[13] above one Kelvin as a key step toward quantum integrated circuits.[14−16]

In it is natural form, germanium contains only 7.76% isotopes with nonzero nuclear spin and, like silicon, can be isotopically enriched[17] to eliminate nuclear spin dephasing. Recent advances in materials science enabled high mobility strained planar germanium (Ge/SiGe) heterostructures[18] for the fabrication of stable gate-defined quantum dots that can confine holes,[19] which are predicted to have a multitude of favorable properties for quantum control.[21,22] The inherent strong spin−orbit coupling of holes allows for fast qubit control[23−25] without integrating external components that complicate scalability, such as nanomagnets and microwave antennas. Moreover, holes do not suffer from valley degeneracy and their small effective mass of $m_h^* = 0.05\ m_e^*$[26] gives rise to large orbital splittings at the band center. These beneficial aspects thereby position holes in germanium as a promising material for quantum information.[27]

While it has been demonstrated that both single- and multihole qubits can be coherently controlled and read out in planar germanium,[25,28] an open question remains which hole occupancy is most advantageous for quantum operation. Electron spin qubits in silicon have been operated with

Received: June 22, 2020
Revised: August 24, 2020
Published: August 24, 2020

https://dx.doi.org/10.1021/acs.nanolett.0c02589
Nano Lett. 2020, 20, 7237−7242

quantum dots containing one, three, and even more electrons with more electrons typically performing favorably in terms of driving speed when driven electrically due to greater wave function mobility.[29,30] Here, we focus on single and multihole spin qubit operation in germanium and concentrate on two critical elements for quantum information with quantum dots: the spin relaxation time and the qubit addressability. We find that both the spin relaxation times of the single-hole ($T_{1,|n=1\rangle}$) and five-hole ($T_{1,|n=5\rangle}$) qubits are long with the longest relaxation time for single-holes measured to be $T_{1,|n=1\rangle} = 32$ ms. Furthermore, we observe that single and multihole qubits exhibit a strong but comparable resonance frequency dependence on electric gate voltage. Interestingly, we find that while the qubit resonance frequency can be significantly tuned with the corresponding plunger gate, it is only weakly dependent on neighbor plunger gates. We thereby conclude that hole spin qubits can be locally addressed, crucial for the operation of dense qubit arrays.

The experiments are performed on a two-dimensional 2 × 2 quantum dot array fabricated using a multilayer gate stack[20] (see Figure 1a). Four plunger gates P_{1-4} define four quantum dots, whose interdot tunnel couplings are controllable via barrier gates B_{12-41}. Four metallic reservoirs O_{1-4} can be controllably coupled to each quantum dot via their respective barrier gates RB_{1-4}. We operate in a configuration whereby electrostatic gates P_1, B_{12}, and P_2 define one large quantum dot, serving as single-hole transistor (SHT) for charge sensing, shown in Figure 1b. By connecting an inductor of $L \approx 2$ μH inline with the ohmic O_1, we form a resonant tank circuit at a frequency of $f_{O1} = 150.7$ MHz used for fast rf charge sensing.[31,32] To optimize the reflection signal and minimize the inline resistance, we use a superconducting inductor made out of NbTiN. A second inline inductance connected to ohmic O_3 makes the device reconfigurable for any of the four double quantum dot-sensor combinations with a second tank circuit resonance at $f_{O3} = 143.3$ MHz. The reflected signal response to rf power delivered to the sample in a frequency range encompassing these two resonances is shown in Figure 1b. Modulation of the channel resistance due to Coulomb oscillations in the SHT is shown in Figure 1c. Next, we apply voltages to the plunger gates P_3 and P_4 to form quantum dots that load via the reservoir barriers RB_3 and RB_4, respectively. By applying sawtooth wave pulses to the plunger gates and simultaneously applying the inverse pulses to the SHT plunger gates P_1 and P_2, we can tune up the device to a double quantum dot of arbitrary occupancy while compensating the charge sensor in real time.

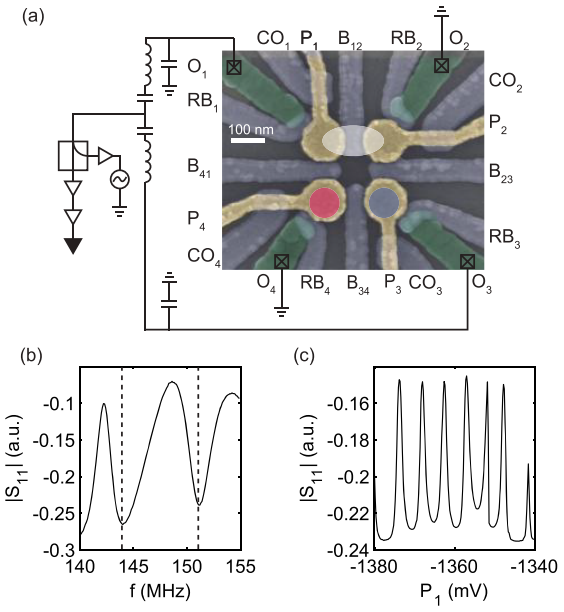

Figure 1. (a) Colored scanning electron microscope image of a nominally identical 2 × 2 quantum dot array. Each quantum dot is defined by a plunger gate, P_{1-4} (yellow) and barrier gates B_{12-41} (blue) are used to set the tunnel coupling. In addition, each quantum dot is coupled to a reservoir, O_{1-4} (green), via a barrier gate RB_{1-4}. A cut off gate, CO_{1-4}, is present for good confinement of the quantum dots. Ohmics 1 and 3 are bonded to an inductor to create a tank circuit with the parasitic capacitance of the device to ground. A radiofrequency tone is applied to the ohmics and the reflected signal $|\Delta S_{11}|$ returns via a directional coupler and is read out. (b) Reflected signal of the two tank circuits. Two clear resonances occur at $f_{O1} = 150.7$ MHz and $f_{O3} = 143.3$ MHz for tank circuits connected to ohmics O_1 and O_3 respectively. (c) Single-hole transistor (SHT) Coulomb oscillations measured in the tank circuit response by applying a microwave tone of 150.7 MHz. A sensing quantum dot is formed underneath the plunger gates P_1 and P_2, by opening the interdot barrier gate B_{12}.

Figure 2a shows the charge stability diagram for a sweep of gates P_3 versus P_4 over the first few charge addition lines in each quantum dot. We focus on the set of anticrossings for the first charge addition line of the quantum dot under P_3 of the form $(N_{P_3},N_{P_4}) \Leftrightarrow (N_{P_3} - 1,N_{P_4} + 1)$, where $N_{P_{3(4)}}$ is the charge occupation of the quantum dot formed under $P_{3(4)}$ from double dot occupation $(1,0) \Leftrightarrow (0,1)$ to $(1,5) \Leftrightarrow (0,6)$. We define a virtual gate space in detuning V_ϵ and energy V_U through a linear transformation of the gate voltages on P_3 and P_4. We apply sawtooth wave pulses that sweep V_ϵ from −2 mV to +2 mV and steps V_U from −2.5 mV to +2.5 mV with respect to the anticrossing. Figure 2b−g shows the resulting stability diagrams.

Pauli spin blockade is observed for $(N_{odd},N_{odd}) \Leftrightarrow (N_{even},N_{even})$ type transitions up to the sixth occupancy. This is consistent with a Fock-Darwin level filling observed for electrons in gallium arsenide[33] and holes in silicon[34] until the same charge occupancy. Working now with the $(1,5) \Leftrightarrow (0,6)$ anticrossing, we extract a lever arm $\alpha = 0.18$ from the thermally broadened polarization line using a hole temperature of 100 mK, which allows us to extract the tunnel couplings.[35] Figure 2h,i shows the used pulse scheme and measured trace. The interdot coupling is kept constant within $t_c = 2.5 \pm 0.2$ GHz for all measurements. In Figure 2j,k,l, we show the relevant pulse sequences in both energy-detuning and virtual gate space, as well as the resulting traces for Pauli spin blockade (PSB) readout, respectively. Each pulse contains an initialization (I), load (L), and read (R) phase. Here we compare the partially blocked (red) and unblocked (dark blue) signals, allowing us to distinguish between the spin up and spin down states in the lower energy quantum dot. The small decay at the beginning of the unblocked trace is due to ringing in the AWG pulses. By loading a hole in P_3 with a random spin state, we expect to observe a blocked signal approximately half of the time. Monitoring the readout signal in the charge sensor as a function of time provides us with the spin relaxation at the readout position, which we find to be $T_{ST} = 103$ μs.

We now assess the spin relaxation of the single- and five-hole qubits. All experiments were performed at a magnetic field $B =$

https://dx.doi.org/10.1021/acs.nanolett.0c02589
Nano Lett. 2020, 20, 7237−7242

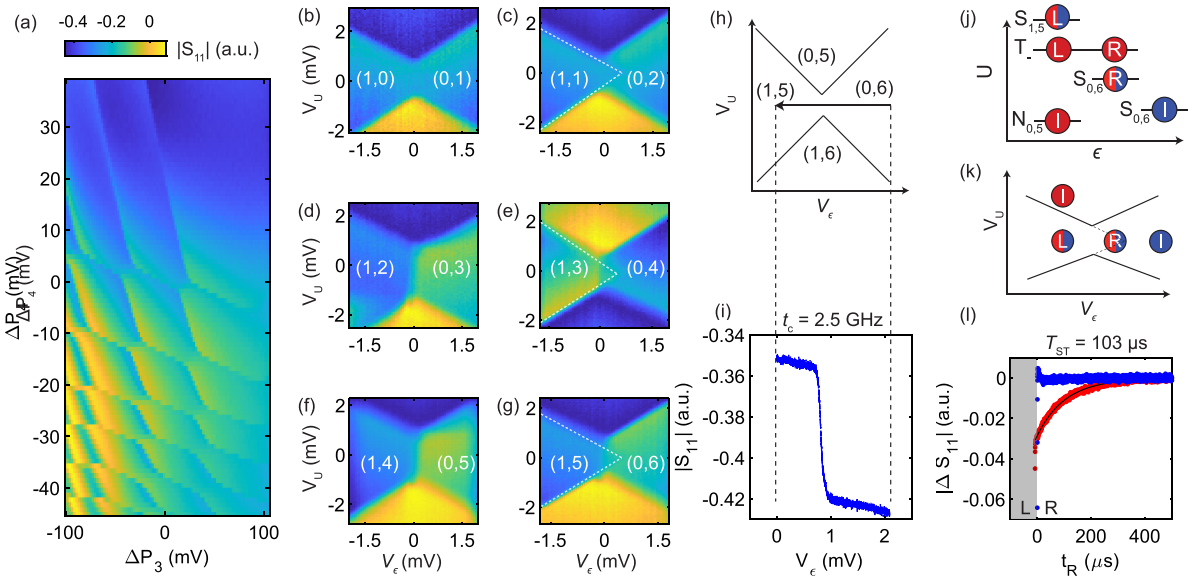

Figure 2. (a) Double quantum dot charge stability diagram obtained by rf-charge sensing in a reconfigurable quadruple quantum dot. A double quantum dot is formed under P_3 (blue) and P_4 (red) with controllable interdot tunnel coupling by tuning interdot barrier gate B_{34} and using rf-charge sensing we can clearly monitor the charge occupancy. The map is taken with 2000 averages. (b−g) Charge stability diagrams of charge anticrossings $(1,N-1) \Leftrightarrow (0,N)$ for integer steps in N from 1 to 6. When N is odd (b,d,f), no spin blockade is present in the transitions. For even N (c,e,g), we observe spin blockade evidenced by triangular extensions of the charge addition lines (white lines are drawn in as a visual guide). (h,i) Interdot tunnel coupling measurement for the $(1,5) \Leftrightarrow (0,6)$ transition. Sweep direction is negative in detuning axis to avoid spin blockade artifacts in spectrum. A tunnel coupling of $t_c = 2.5$ GHz is obtained and kept within 200 MHz of this value for all measurements in the work. (j) Cartoon of the initialization (I), loading (L), and readout (R) points of our pulse sequences in detuning ϵ and energy U space. The blue sequence loads the $|S_{(1,5)}\rangle$ singlet state which is not blocked on readout. The red sequence initializes in the (0,5) charge state $N_{0,5}$ and loads a randomly oriented spin resulting in the singlet state or triplet state with equal probability (red), the latter of which results in a blocked signal. (k) Pulse sequences as a function of virtual detuning (V_ϵ) and energy (V_U) gates for the case of loading a singlet state (blue) and triplet/singlet state with equal probability (red). (l) Readout traces showing the signal difference between the spin blocked (red) and unblocked (blue) signals as a function of time spent in the read phase (t_R). Each trace is averaged 1000 times. The small deviation in the blue trace around $t_R = 0$ μs is due to ringing in the applied AWG pulse. Loading a random spin under P_3 (red) leads to a singlet−triplet decay time of $T_{ST} = 103$ μs.

0.67 T, allowing for a comparison with previous germanium hole spin qubit experiments[25,28] in a similar magnetic field regime. The Zeeman energy difference between our qubits manifests from spin−orbit induced changes in the g-factor of each qubit, lifting the antiparallel spin state energy degeneracy when an external magnetic field is applied. Figure 3a shows the pulse sequences used to measure the spin relaxation times of the hole spins in each quantum dot. Each pulse sequence consists of an initialization (I), load (L), and read (R) phase with two ramps between the I and L phases (t_{IL}), and the L and R phases (t_{LR}). Using the first two sequences (red and blue in Figure 3a) a randomly orientated spin is loaded into the quantum dot defined under P_4 or P_3 respectively. The red and blue pulse sequences also contain an extra wait (W) step before initialization in the (1,5) charge state to relax the spins to their ground state. This allows deterministic probing of the spin relaxation time of each dot, by varying the load wait time t_L.

The third pulse sequence (yellow in Figure 3a) initializes the system in the singlet state with charge configuration $(N_{P3}, N_{P4}) = (0,6)$ $(|S_{(0,6)}\rangle)$. The system is then tuned to the charge configuration $(N_{P3}, N_{P4}) = (1,5)$ $(|S_{(1,5)}\rangle)$. We pulse with a ramp time $t_{IL} = 100$ ns, resulting in a diabatic movement through the charge anticrossing, and through fast charge relaxation we expect to initialize the $|\uparrow, \downarrow\rangle$ and $|\downarrow, \uparrow\rangle$ states randomly with equal probability. This initialization then allows us to efficiently measure both spin relaxation times in a single measurement, since the readout signal is a linear combination of both spin relaxation decays and is useful since it allows for fast measurements even when the quantum dot-reservoir couplings are low. Upon readout, the inherent spin orbit coupling in our system results in an avoided crossing between the $|T_-\rangle$ and $|S_{(0,6)}\rangle$ states, potentially limiting our readout fidelity. We therefore minimize the ramp time and operate with $t_{LR} = 100$ ns.

In Figure 3b, we show the spin relaxation times of the quantum dots using the three sequences. We find $T_{1,|n=5\rangle} = 1.0$ ms and $T_{1,|n=1\rangle} = 4.23$ ms by fitting exponential decays to the individual measurements. The measurement corresponding to the sequence by randomly preparing a spin up state in one of the two quantum dots is fitted with a double exponential curve using the time constants of the individual decays, and we have left the amplitudes and asymptotes as free fitting parameters. We find approximately equal amplitudes for each decay, corresponding with an equal loading of both antiparallel spin states.

We can further increase the single-hole relaxation time by reducing the quantum dot-reservoir coupling. Using the barrier gate RB_3, we tune the quantum dot-reservoir coupling of the single-hole quantum dot from 81.43 to 27.45 kHz (see Supporting Information Section I). We note that these dot-reservoir couplings do not represent the actual tunnelling times at the point of measurement, which are expected to be orders of magnitude longer. The spin relaxation decay shown in Figure 3c has been analyzed using the above-mentioned double exponential fit and we find an significantly increased

https://dx.doi.org/10.1021/acs.nanolett.0c02589
Nano Lett. 2020, 20, 7237−7242

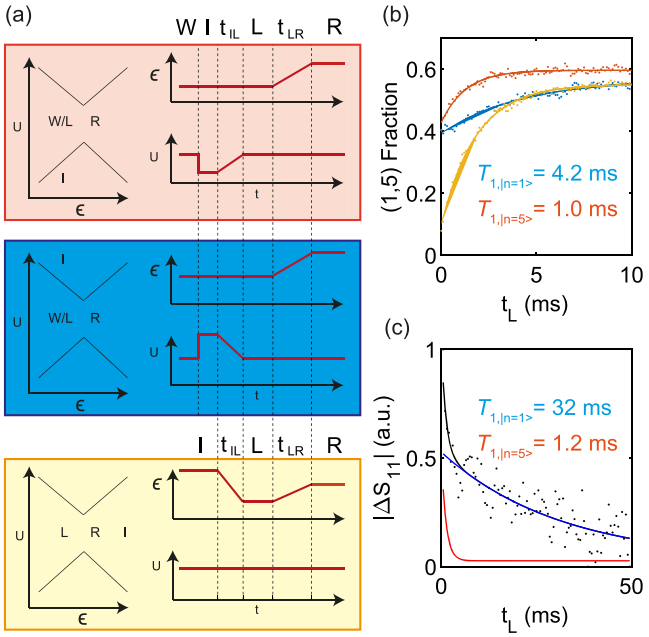

Figure 3. (a) Pulse sequences utilized for different loading protocols. Red loads a random spin in P_4, blue loads a random spin in P_3, and yellow loads either the $|S_{(1,5)}\rangle$ or a mixture of $|S_{(1,5)}\rangle$ and $|T_0\rangle$ depending on the adiabaticity of the IL pulse. (b) Deterministic loading of a single-hole in P_4 and P_3 (red, blue, respectively) and mixed state loading (yellow). We extract spin relaxation times of $T_{1,|n=5\rangle}$ = 1.0 ms and $T_{1,|n=1\rangle}$ 4.23 ms for each deterministically loaded quantum dot, which we fit as a double exponential for the mixed loading case. (c) Longest spin relaxation trace taken after minimizing reservoir-dot tunnel coupling. We extract two spin relaxation times of $T_{1,|n=1\rangle}$ = 32 ms and $T_{1,|n=5\rangle}$ = 1.2 ms.

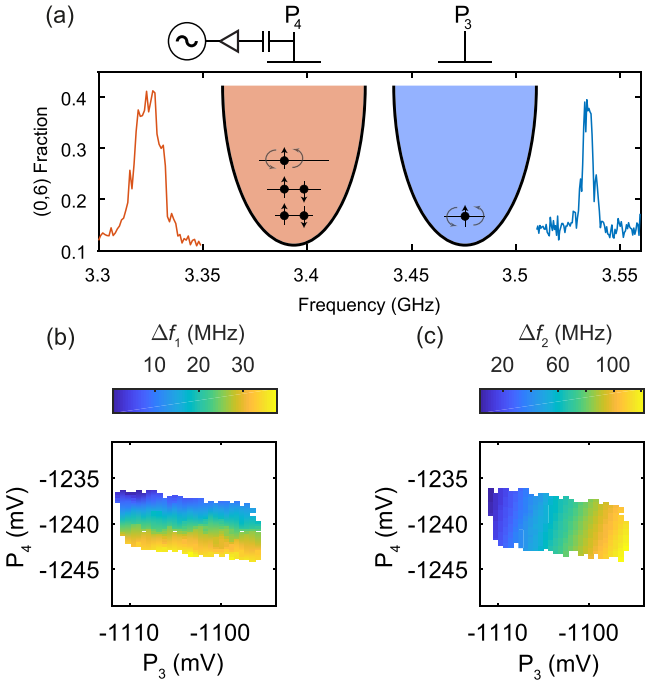

Figure 4. (a) Qubit resonance frequency of the five-hole (3.33 GHz) and single-hole qubit (3.53 GHz). The magnetic field is set to B = 667 mT. A microwave tone is applied to the gate P_4, which drives both hole spins, as indicated by the cartoon inset. We extract in-plane g-factors of $g_{|n=1\rangle}$ = 0.362 and $g_{|n=5\rangle}$ = 0.383 for plunger gate values P_3 = 1098 mV, P_4 = 1236 mV. (b) Five-hole (f_1) and (c) single-hole (f_2) resonance frequency dependence on gate voltage. We find a strong dependence of the resonance frequency on the respective plunger gate but a significantly reduced dependence on the neighboring plunger gate voltage.

single-hole spin relaxation time $T_{1,|n=1\rangle}$ = 32 ms. By limiting the dot-reservoir tunnel coupling, we have demonstrated spin relaxation lifetimes significantly longer than results previously reported for planar germanium quantum dots ($T_{1,|n=1\rangle}$ = 1.2 ms[28]), hut wires (T_1 = 90 μs[36]), nanowires (T_1 = 600 μs[37]), and even holes in gallium arsenide (T_1 = 60 μs[38]) and silicon (T_1 = 8.3 μs[39]) at similar magnetic fields. We expect that the main cause for the observation of longer spin relaxation times for single-hole spins compared to many hole spins originates from the tighter confinement of the quantum dot under P_3. This leads to larger energy splittings to the excited states, a smaller degree of capacitive coupling to electrical fluctuations, and a smaller dot-reservoir coupling. Additionally, further reduction of the dot-reservoir tunnel coupling would likely improve the multihole spin relaxation time. Further investigation into the magnetic field dependence of T_1 could produce information about the spin relaxation mechanisms present and yield insights into means of further optimizing T_1. However, our demonstration of T_1 up to 32 ms shows encouraging spin relaxation times for quantum information processing, and that spin states in planar germanium define the benchmark for spin relaxation in hole-based quantum dots.

The presence of spin−orbit coupling allows for electrical and coherent control of the spin states without the need for additional structures such as striplines or micromagnets.[21,22,24,25] We investigate the individual tunability and addressability of the single- and multihole qubits. In Figure 4a, we show results where we have applied a microwave tone of length t_{mw} = 400 ns to the gate P_4. We observe two resonance frequencies at 3.33 and 3.53 GHz in Figure 4a, corresponding to an in-plane Zeeman energy difference ΔE_z = 200 MHz, as a result of the spin−orbit induced g-factor difference between each qubit. The difference in peak width is due to the delivery of microwave power via plunger gate P_4, resulting in a power broadened resonance line width with respect to that of the spin under P_3. Figure 4b,c shows the dependence of each resonance frequency on the electrostatic gate voltages on the two relevant plunger gates P_3 and P_4. We initialize in the $|S_{(0,6)}\rangle$ singlet state, then load in different points in the (1,5) charge state by changing the potentials applied to P_3 and P_4. We then manipulate the spins by applying a microwave tone to P_4 and read out in the PSB window. The mechanism by which our resonance frequency changes is due to the modulation of the spin−orbit interaction via change in local electric fields, leading to a modulation of the g-factor of each qubit. The resonance frequency dependence on gate voltage is approximately linear. For the five-hole qubit we find a dependence on its plunger gate voltage df_1/dP_4 = −4.78 MHz/mV and we find df_1/dP_3 = −0.155 MHz/mV. For the single-hole qubit, we find a slightly stronger dependence on its plunger gate voltage df_2/dP_3 = 6.78 MHz/mV and we find a cross talk df_2/dP_4 = −1.79 MHz/mV. These values are comparable to those measured in a previous work on the same device under different electrostatic tuning parameters, and therefore we expect the coherence times of each qubit to be on the order of 300 ns as measured earlier.[28] This corresponds to a cross talk ratio of about 1:30 for the five-hole qubit and about 1:4 for the single-hole qubit. The cross talk for the single-hole qubit is comparable to the

https://dx.doi.org/10.1021/acs.nanolett.0c02589
Nano Lett. 2020, 20, 7237−7242

lever arm ratio (see Supporting Information Section II) $\alpha_{P_3/P_4}(f_2) = 0.11$. Remarkably, the five-hole qubit has a lever arm ratio $\alpha_{P_4/P_3}(f_1) = 0.07$, significantly larger than the resonance frequency cross talk ratio.

In summary, we have demonstrated benchmarks for spin relaxation in hole quantum dots and found $T_{1,|n=1\rangle} = 32$ ms for a single-hole qubit and $T_{1,|n=5\rangle} = 1.2$ ms for a five-hole qubit and conclude that spin relaxation is not a bottleneck for quantum computation with holes. We have shown the presence of Pauli-spin blockade at different hole fillings and have found it to be consistent with a Fock-Darwin spectrum that only involves spin degeneracy. We find that both the single-hole and multihole qubit resonance frequency can be tuned over a large range. We find that the resonance frequencies are only weakly dependent on neighboring gates, which result in good local addressability. The observation of the sign difference in the resonance frequency dependence on gate voltage and the strength of the cross talk ratio of the resonance frequencies may provide insight in the nature of the driving mechanism of holes in planar germanium. This is relevant for future work, and a possible scenario is that the reduced cross talk of the five-hole qubit originates from an increased heavy-hole light-hole mixing. Such a change may affect the qubit resonance frequency dependence on the amplitude and orientation of the electric field, but further research is needed to investigate this. The long spin lifetimes and excellent individual qubit addressability are encouraging for the operation of hole qubits positioned in large two-dimensional arrays.

■ ASSOCIATED CONTENT

Supporting Information

The Supporting Information is available free of charge at https://pubs.acs.org/doi/10.1021/acs.nanolett.0c02589.

Methods used to extract dot-reservoir tunnel coupling, as well as the virtual gate matrices used (PDF)

■ AUTHOR INFORMATION

Corresponding Authors

W. I. L. Lawrie − *QuTech and Kavli Institute of Nanoscience, Delft University of Technology, 2628 CJ Delft, The Netherlands;* orcid.org/0000-0002-9946-4117; Email: w.i.l.lawrie@tudelft.nl

M. Veldhorst − *QuTech and Kavli Institute of Nanoscience, Delft University of Technology, 2628 CJ Delft, The Netherlands;* Email: m.veldhorst@tudelft.nl

Authors

N. W. Hendrickx − *QuTech and Kavli Institute of Nanoscience, Delft University of Technology, 2628 CJ Delft, The Netherlands;* orcid.org/0000-0003-4224-7418

F. van Riggelen − *QuTech and Kavli Institute of Nanoscience, Delft University of Technology, 2628 CJ Delft, The Netherlands*

M. Russ − *QuTech and Kavli Institute of Nanoscience, Delft University of Technology, 2628 CJ Delft, The Netherlands*

L. Petit − *QuTech and Kavli Institute of Nanoscience, Delft University of Technology, 2628 CJ Delft, The Netherlands;* orcid.org/0000-0001-9877-3623

A. Sammak − *QuTech and Netherlands Organization for Applied Scientific Research, TNO, 2628 CK Delft, The Netherlands*

G. Scappucci − *QuTech and Kavli Institute of Nanoscience, Delft University of Technology, 2628 CJ Delft, The Netherlands;* orcid.org/0000-0003-2512-0079

Complete contact information is available at: https://pubs.acs.org/10.1021/acs.nanolett.0c02589

Notes

The authors declare no competing financial interest.

All data underlying this study are available from the 4TU ResearchData repository at https://doi.org/10.4121/12849800.

■ ACKNOWLEDGMENTS

The authors acknowledge support through a FOM Projectruimte and through a Vidi programme, both associated with The Netherlands Organisation for Scientific Research (NWO).

■ REFERENCES

(1) Loss, D.; DiVincenzo, D. P. Quantum computation with quantum dots. *Phys. Rev. A: At., Mol., Opt. Phys.* **1998**, *57*, 120−126.

(2) Petta, J. R.; Johnson, A. C.; Taylor, J. M.; Laird, E. A.; Yacoby, A.; Lukin, M. D.; Marcus, C. M.; Hanson, M. P.; Gossard, A. C. Coherent Manipulation of Electron Spins in Semiconductor Quantum Dots. *Science* **2005**, *309*, 2180−2184.

(3) Koppens, F. H.; Buizert, C.; Tielrooij, K. J.; Vink, I. T.; Nowack, K. C.; Meunier, T.; Kouwenhoven, L. P.; Vandersypen, L. M. Driven coherent oscillations of a single electron spin in a quantum dot. *Nature* **2006**, *442*, 766−771.

(4) Itoh, K. M.; Watanabe, H. Isotope engineering of silicon and diamond for quantum computing and sensing applications. *MRS Commun.* **2014**, *4* (4), 143−157.

(5) Veldhorst, M.; Hwang, J. C.; Yang, C. H.; Leenstra, A. W.; De Ronde, B.; Dehollain, J. P.; Muhonen, J. T.; Hudson, F. E.; Itoh, K. M.; Morello, A.; Dzurak, A. S. An addressable quantum dot qubit with fault-tolerant control-fidelity. *Nat. Nanotechnol.* **2014**, *9*, 981−985.

(6) Yang, C. H.; Rossi, A.; Ruskov, R.; Lai, N. S.; Mohiyaddin, F. A.; Lee, S.; Tahan, C.; Klimeck, G.; Morello, A.; Dzurak, A. S. Spin-valley lifetimes in a silicon quantum dot with tunable valley splitting. *Nat. Commun.* **2013**, *4*, 1−8.

(7) Yang, C. H.; Chan, K. W.; Harper, R.; Huang, W.; Evans, T.; Hwang, J. C.; Hensen, B.; Laucht, A.; Tanttu, T.; Hudson, F. E.; Flammia, S. T.; Itoh, K. M.; Morello, A.; Bartlett, S. D.; Dzurak, A. S. Silicon qubit fidelities approaching incoherent noise limits via pulse engineering. *Nature Electronics* **2019**, *2*, 151−158.

(8) Yoneda, J.; Takeda, K.; Otsuka, T.; Nakajima, T.; Delbecq, M. R.; Allison, G.; Honda, T.; Kodera, T.; Oda, S.; Hoshi, Y.; Usami, N.; Itoh, K. M.; Tarucha, S. A quantum-dot spin qubit with coherence limited by charge noise and fidelity higher than 99.9%. *Nat. Nanotechnol.* **2018**, *13*, 102−106.

(9) Veldhorst, M.; Yang, C. H.; Hwang, J. C. C.; Huang, W.; Dehollain, J. P.; Muhonen, J. T.; Simmons, S.; Laucht, A.; Hudson, F. E.; Itoh, K. M.; Morello, A.; Dzurak, A. S. A two-qubit logic gate in silicon. *Nature* **2015**, *526*, 410−414.

(10) Zajac, D. M.; Sigillito, A. J.; Russ, M.; Borjans, F.; Taylor, J. M.; Burkard, G.; Petta, J. R. Resonantly driven CNOT gate for electron spins. *Science* **2018**, *359*, 439−442.

(11) Watson, T. F.; Philips, S. G.; Kawakami, E.; Ward, D. R.; Scarlino, P.; Veldhorst, M.; Savage, D. E.; Lagally, M. G.; Friesen, M.; Coppersmith, S. N.; Eriksson, M. A.; Vandersypen, L. M. A programmable two-qubit quantum processor in silicon. *Nature* **2018**, *555*, 633−637.

(12) Yang, C. H.; Leon, R. C. C.; Hwang, J. C. C.; Saraiva, A.; Tanttu, T.; Huang, W.; Lemyre, J. C.; Chan, K. W.; Tan, K. Y.; Hudson, F. E.; Itoh, K. M.; Morello, A.; Pioro-Ladrière, M.; Laucht, A.; Dzurak, A. S. Silicon quantum processor unit cell operation above one Kelvin. *Nature* **2020**, *580*, 350−354.

(13) Petit, L.; Eenink, H. G. J.; Russ, M.; Lawrie, W. I. L.; Hendrickx, N. W.; Clarke, J. S.; Vandersypen, L. M. K.; Veldhorst, M. Universal quantum logic in hot silicon qubits. *Nature* **2020**, *580*, 355−359.
(14) Vandersypen, L. M. K.; Bluhm, H.; Clarke, J. S.; Dzurak, A. S.; Ishihara, R.; Morello, A.; Reilly, D. J.; Schreiber, L. R.; Veldhorst, M. Interfacing spin qubits in quantum dots and donors - hot, dense and coherent. *npj Quantum Information* **2017**, *3*, 34.
(15) Veldhorst, M.; Eenink, H. G.; Yang, C. H.; Dzurak, A. S. Silicon CMOS architecture for a spin-based quantum computer. *Nat. Commun.* **2017**, *8*, 1766.
(16) Li, R.; Petit, L.; Franke, D. P.; Dehollain, J. P.; Helsen, J.; Steudtner, M.; Thomas, N. K.; Yoscovits, Z. R.; Singh, K. J.; Wehner, S.; Vandersypen, L. M.; Clarke, J. S.; Veldhorst, M. A crossbar network for silicon quantum dot qubits. *Science Advances* **2018**, *4*, No. eaar3960.
(17) Itoh, K.; Haller, E. E.; Hansen, W. L.; Farmer, J. W.; Ozhogin, V. I.; Rudnev, A.; Tikhomirov, A. High purity isotopically enriched 70Ge and 74Ge single crystals: Isotope separation, growth, and properties. *J. Mater. Res.* **1993**, *8*, 1341−1347.
(18) Sammak, A.; Sabbagh, D.; Hendrickx, N. W.; Lodari, M.; Paquelet Wuetz, B.; Tosato, A.; Yeoh, L. R.; Bollani, M.; Virgilio, M.; Schubert, M. A.; Zaumseil, P.; Capellini, G.; Veldhorst, M.; Scappucci, G. Shallow and Undoped Germanium Quantum Wells: A Playground for Spin and Hybrid Quantum Technology. *Adv. Funct. Mater.* **2019**, *29*, 1807613.
(19) Hendrickx, N. W.; Franke, D. P.; Sammak, A.; Kouwenhoven, M.; Sabbagh, D.; Yeoh, L.; Li, R.; Tagliaferri, M. L.; Virgilio, M.; Capellini, G.; Scappucci, G.; Veldhorst, M. Gate-controlled quantum dots and superconductivity in planar germanium. *Nat. Commun.* **2018**, *9*, 2835.
(20) Lawrie, W. I. L.; et al. Quantum Dot Arrays in Silicon and Germanium. *Appl. Phys. Lett.* **2020**, *116*, 080501.
(21) Bulaev, D. V.; Loss, D. Spin relaxation and decoherence of holes in quantum dots. *Phys. Rev. Lett.* **2005**, *95*, 076805.
(22) Bulaev, D. V.; Loss, D. Electric dipole spin resonance for heavy holes in quantum dots. *Phys. Rev. Lett.* **2007**, *98*, 097202.
(23) Maurand, R.; Jehl, X.; Kotekar-Patil, D.; Corna, A.; Bohuslavskyi, H.; Laviéville, R.; Hutin, L.; Barraud, S.; Vinet, M.; Sanquer, M.; De Franceschi, S. A CMOS silicon spin qubit. *Nat. Commun.* **2016**, *7*, 13575.
(24) Watzinger, H.; Kukučka, J.; Vukušić, L.; Gao, F.; Wang, T.; Schäffler, F.; Zhang, J. J.; Katsaros, G. A germanium hole spin qubit. *Nat. Commun.* **2018**, *9*, 3902.
(25) Hendrickx, N. W.; Franke, D. P.; Sammak, A.; Scappucci, G.; Veldhorst, M. Fast two-qubit logic with holes in germanium. *Nature* **2020**, *577*, 487−491.
(26) Lodari, M.; Tosato, A.; Sabbagh, D.; Schubert, M. A.; Capellini, G.; Sammak, A.; Veldhorst, M.; Scappucci, G. Light effective hole mass in undoped Ge/SiGe quantum wells. *Phys. Rev. B: Condens. Matter Mater. Phys.* **2019**, *100*, 041304.
(27) Scappucci, G.; Kloeffel, C.; Zwanenburg, F. A.; Loss, D.; Myronov, M.; Zhang, J.-J.; De Franceschi, S.; Katsaros, G.; Veldhorst, M. *germanium quantum information route*. 2020, arXiv:2004.08133 (accessed August 22, 2020).
(28) Hendrickx, N. W.; Lawrie, W. I. L.; Petit, L.; Sammak, A.; Scappucci, G.; Veldhorst, M. A single-hole spin qubit. *Nat. Commun.* **2020**, *11*, 6.
(29) Veldhorst, M.; Ruskov, R.; Yang, C. H.; Hwang, J. C. C.; Hudson, F. E.; Flatte, M. E.; Tahan, C.; Itoh, K. M.; Morello, A.; Dzurak, A. S. Spin-orbit coupling and operation of multivalley spin qubits. *Phys. Rev. B: Condens. Matter Mater. Phys.* **2015**, *92*, No. 201401.
(30) Leon, R. C.; Yang, C. H.; Hwang, J. C.; Lemyre, J. C.; Tanttu, T.; Huang, W.; Chan, K. W.; Tan, K. Y.; Hudson, F. E.; Itoh, K. M.; Morello, A.; Laucht, A.; Pioro-Ladrière, M.; Saraiva, A.; Dzurak, A. S. Coherent spin control of s-, p-, d- and f-electrons in a silicon quantum dot. *Nat. Commun.* **2020**, *11*, 1−7.
(31) Schoelkopf, R. J.; Wahlgren, P.; Kozhevnikov, A. A.; Delsing, P.; Prober, D. E. The radio-frequency single-electron transistor (RF-SET): A fast and ultrasensitive electrometer. *Science* **1998**, *280*, 1238−1242.
(32) Vukušić, L.; Kukučka, J.; Watzinger, H.; Katsaros, G. Fast Hole Tunneling Times in Germanium Hut Wires Probed by Single-Shot Reflectometry. *Nano Lett.* **2017**, *17*, 5706−5710.
(33) Tarucha, S.; Austing, D. G.; Honda, T.; van der Hage, R. J.; Kouwenhoven, L. P. Shell filling and spin effects in a few electron quantum dot. *Phys. Rev. Lett.* **1996**, *77*, 3613−3616.
(34) Liles, S. D.; Li, R.; Yang, C. H.; Hudson, F. E.; Veldhorst, M.; Dzurak, A. S.; Hamilton, A. R. Spin and orbital structure of the first six holes in a silicon metal-oxide-semiconductor quantum dot. *Nat. Commun.* **2018**, *9*, 1−7.
(35) DiCarlo, L.; Lynch, H. J.; Johnson, A. C.; Childress, L. I.; Crockett, K.; Marcus, C. M.; Hanson, M. P.; Gossard, A. C. Differential charge sensing and charge delocalization in a tunable double quantum dot. *Phys. Rev. Lett.* **2004**, *92*, 226801.
(36) Vukušić, L.; Kukučka, J.; Watzinger, H.; Milem, J. M.; Schäffler, F.; Katsaros, G. Single-Shot Readout of Hole Spins in Ge. *Nano Lett.* **2018**, *18*, 7141−7145.
(37) Hu, Y.; Kuemmeth, F.; Lieber, C. M.; Marcus, C. M. Hole spin relaxation in Ge-Si core-shell nanowire qubits. *Nat. Nanotechnol.* **2012**, *7*, 47−50.
(38) Bogan, A.; Studenikin, S.; Korkusinski, M.; Gaudreau, L.; Zawadzki, P.; Sachrajda, A.; Tracy, L.; Reno, J.; Hargett, T. single-hole spin relaxation probed by fast single-shot latched charge sensing. *Communications Physics* **2019**, *2*, 1−8.
(39) Bohuslavskyi, H.; Kotekar-Patil, D.; Maurand, R.; Corna, A.; Barraud, S.; Bourdet, L.; Hutin, L.; Niquet, Y. M.; Jehl, X.; De Franceschi, S.; Vinet, M.; Sanquer, M. Pauli blockade in a few-hole PMOS double quantum dot limited by spin-orbit interaction. *Appl. Phys. Lett.* **2016**, *109*, 193101.

https://dx.doi.org/10.1021/acs.nanolett.0c02589
Nano Lett. 2020, 20, 7237−7242